Statistical properties of wave kinematics in long-crested irregular waves propagating over non-uniform bathymetry

C. Lawrence,[1] K. Trulsen,[1, a)] and O. Gramstad[2]
[1)]*Department of Mathematics, University of Oslo, 0371 Oslo, Norway*
[2)]*Group Technology and Research, DNV GL, 1322 Høvik, Norway*

(Dated: 17 March 2021)

Experimental and numerical evidence have shown that non-uniform bathymetry may alter significantly the statistical properties of surface elevation in irregular wave fields. The probability of 'rogue' waves is increased near the edge of the upslope as long-crested irregular waves propagate into shallower water. The present paper studies the statistics of wave kinematics in long-crested irregular waves propagating over a shoal with a Monte-Carlo approach. High Order Spectral Method is employed as wave propagation model and Variational Boussinesq Model is employed to calculate wave kinematics. The statistics of horizontal fluid velocity can be different from statistics in surface elevation as the waves propagate over uneven bathymetry. We notice strongly non-Gaussian statistics when the depth changes abruptly in sufficiently shallow water. We find an increase of kurtosis in the horizontal velocity around the downslope area. Furthermore, the effects of the bottom slope with different incoming waves are discussed in terms of kurtosis and skewness. Finally, we investigate the evolution of kurtosis and skewness of the horizontal velocity over a sloping bottom in a deeper regime. The vertical variation of these statistical quantities is also presented.

Key words: surface waves, wave kinematics, wave statistics

I. INTRODUCTION

Ship and offshore structures are exposed to ocean waves where ship motions and wave-induced loads are directly connected with water particle velocities[1,2]. In a finite depth regime, wave kinematics affect the sediment transport at the seabed and may cause scour around a structure such as a pile[3]. Therefore, statistical analysis with accurate wave kinematics description is demanded in marine design.

The linear theory for water waves with small amplitude over a uniform depth is known as Airy theory. Random sea states with Gaussian statistics can be described as a linear superposition of monochromatic linear waves. This theory is extensively applied in marine engineering for the statistical analysis of random seas[4]. In reality, ocean waves are nonlinear and do not follow Gaussian statistics. Second-order theory was developed as a remedy to the linear Airy solution[5,6]. Other nonlinear effects provoked by bottom variation and higher-order effects such as modulational instability may contribute to deviation from Gaussian statistics.

Deep water waves may have modulational instability under some circumstances, e.g. narrow banded spectrum and sufficiently high amplitude. For flat bottom and deep water waves with the presence of modulational instability, the excess kurtosis of surface elevation was found to be positive in Janssen and Onorato [7]. In contrast, negative excess kurtosis occurred in shallow water with the absence of modulational instability.

Without modulational instability, Ochi [8] showed that Gaussian random waves in deep water can transform to non-Gaussian random waves as they propagate from deep to shallow water. The deviation from Gaussian statistics is more pronounced in shallow water and this shallow water effect is mainly due to second-order effects.

Field experiments reported by Bitner [9] and Cherneva *et al.* [10] suggested that non-uniform bathymetry may alter the statistical properties of surface elevation from Gaussian statistics. In the last decades, there has been a surge of interest in experimental and numerical studies to investigate statistical properties of irregular wave fields with bottom variation.

Trulsen, Zeng, and Gramstad [11] reported laboratory experiments of long-crested irregular waves propagating over a sloping bottom. They found that there can be a local maximum in the skewness and the kurtosis of surface elevation near the edge of the shallower side of the slope. Other laboratory experiments by Ma, Dong, and Ma [12], Kashima, Hirayama, and Mori [13], Bolles, Speer, and Moore [14] and Zhang *et al.* [15] support this finding.

In shallow water regime, Sergeeva, Pelinovsky, and Talipova [16] utilized Korteweg-de Vries model to show that the skewness and kurtosis of wave elevation increase when the depth decreases. Majda, Moore, and Qi [17] developed a statistical model based on truncated KdV-equation and also confirmed the experimental results in Bolles, Speer, and Moore [14]. Motivated by the statistical model of Majda, Moore, and Qi [17], Moore *et al.* [18] conducted new experimental measurements and compared with the truncated KdV model in shallow water with abrupt depth changes.

In intermediate depth, Gramstad *et al.* [19] used a Boussinesq model with improved linear dispersion to confirm the experimental results in Trulsen, Zeng, and Gramstad [11]. Furthermore, it was discovered that for a milder slope, there is no local maximum of statistical quantities in the surface elevation. This finding is supported by Zheng *et al.* [20] with a boundary element method. Another numerical model based on a spectral conforming mapping method was used by Viotti and Dias [21] for a stronger depth transition. Strongly non-Gaussian statistics were observed in a region localized around the depth

[a)]Corresponding author, e-mail : karstent@math.uio.no

transition. This transition region connects two different statistical equilibria.

In deep water regime, Zeng and Trulsen [22] used a nonlinear Schrödinger model for variable depth and did not find any local maximum of skewness and kurtosis in deep water. Instead, the kurtosis decreases toward the shallower domain to achieve a new statistical equilibrium. So far no laboratory experiments have been performed in this depth regime.

A graphical presentation of the different depth regimes can be found in Figure 1 of Trulsen *et al.* [23].

For short-crested waves, Ducrozet and Gouin [24] with the aid of High Order Spectral Method for variable depth found that the enhancement of rogue wave occurence due to a sloping bottom is reduced for a directional wave field. According to the authors knowledge, this is the only numerical simulation that considers the directionality of a random wave field propagating over non-uniform bathymetry for statistical purposes and no laboratory experiments have been done for this case.

All of the experimental and numerical results mentioned above focus on extreme wave statistics enhancement in surface elevation due to wave propagation from deeper to a shallower depth. In Gramstad *et al.* [19], the enhancement of rogue wave occurrence is absent in the case that waves propagating from shallower to deeper water but they did not investigate the statistics of velocity field. It was previously shown that the horizontal velocity also deviates from Gaussian statistics (Tung [25], Cieslikiewicz and Gudmestad [26]) and the deviation can be even stronger in shallower water as pointed out in Song and Wu [27] and Alberello *et al.* [28]. The recent experimental results of long-crested irregular waves over a shoal reported by Trulsen *et al.* [23] showed an increase of kurtosis in the horizontal velocity which is different from the surface elevation. The local maximum of kurtosis of surface elevation occurred near the edge of the slope on the shallower side as expected, meanwhile the local maximum of kurtosis of the horizontal velocity was found over the downward slope on the lee side. This new discovery implies that the rogue waves in surface elevation and horizontal velocity can occur at different locations. This result is relevant for design of offshore structures in regions of shallow and intermediate water depth.

As a continuation of previous works, the present paper employs a numerical model to investigate the statistical properties of horizontal velocity over non-uniform depth. We confirm the experimental result in Trulsen *et al.* [23] and analyze further the effects of different incoming waves and bottom slope. We also extend the evolution of skewness and kurtosis in a deeper regime as discussed in Zeng and Trulsen [22] by including the statistical properties of horizontal velocity.

The organization of the rest of the paper is as follows. In Section II, we describe briefly the numerical models for wave evolution and wave kinematics calculation. The setup for numerical simulations is given in Section III. The numerical results are shown and discussed in Section IV. Finally, the conclusions are given in Section V.

II. NUMERICAL METHOD

A. Wave evolution

A 2D fluid domain, periodic in horizontal direction with length L and a Cartesian coordinate system is considered as shown in Figure 1. Let $z = \eta(x,t)$ denote the free surface elevation with $z = 0$ being the still water level and $z = -h_0 + \mathscr{B}(x)$ the bottom topography, where h_0 is the mean water depth and $\mathscr{B}(x)$ is the bottom variation. Hence, the considered fluid domain becomes : $z \in [-h_0 + \mathscr{B}(x), \eta(x,t)]$ and $x \in [0, L)$.

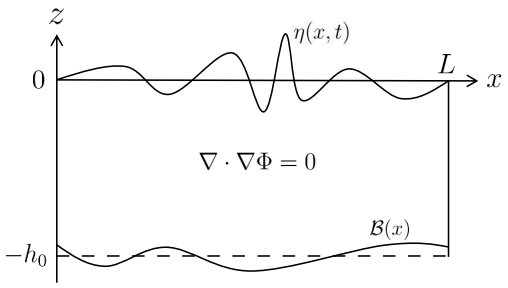

FIG. 1: Description of fluid domain with surface elevation $\eta(x,t)$, mean water depth h_0 and bottom variation $\mathscr{B}(x)$.

Assuming irrotational flow, the fluid velocity can be expressed by the velocity potential Φ, $\vec{V} = \nabla\Phi$. The continuity equation combined with the assumption of an incompressible fluid then becomes the Laplace equation

$$\nabla \cdot \nabla\Phi = 0. \tag{1}$$

As pointed out in Zakharov [29], the dynamic equations for inviscid irrotational nonlinear water waves can be written in Hamiltonian structure with surface elevation $\eta(x,t)$ and surface potential $\phi = \Phi(x, z = \eta, t)$ as canonical variables

$$\begin{aligned} \frac{\partial \eta}{\partial t} &= W\left(1 + \left|\frac{\partial \eta}{\partial x}\right|^2\right) - \frac{\partial \phi}{\partial x}\frac{\partial \eta}{\partial x} \\ \frac{\partial \phi}{\partial t} &= -g\eta - \frac{1}{2}\left|\frac{\partial \phi}{\partial x}\right|^2 + \frac{1}{2}W^2\left(1 + \left|\frac{\partial \eta}{\partial x}\right|^2\right) \end{aligned} \tag{2}$$

where g is the acceleration of gravity and $W = \frac{\partial \Phi}{\partial z}\Big|_{z=\eta}$ is the vertical velocity at the surface. In order to solve the system (2), the vertical velocity at the surface W needs to be evaluated. An efficient pseudo spectral method to calculate the surface vertical velocity W in terms of surface elevation η and surface potential ϕ was initially introduced by Dommermuth and Yue [30] and West *et al.* [31] for flat bottom, and has been known as High Order Spectral Method (HOSM). The extension of HOSM to deal with small variation of bottom was introduced in Liu and Yue [32]. Later, HOSM for varying bottom

was improved by separating the order of nonlinearity for the free surface and for the bottom (see Gouin, Ducrozet, and Ferrant [33,34]). The dynamic equations in (2) can be solved numerically using standard ordinary differential equations solver after applying pseudo spectral formulation. In the present work, we use HOSM for varying bottom by Gouin, Ducrozet, and Ferrant [33] as wave evolution model and a brief summary of the method is presented in the following.

The velocity potential $\Phi(x,z,t)$ is expressed as a truncated power series

$$\Phi(x,z,t) = \sum_{m=1}^{M} \Phi^{(m)}(x,z,t) \tag{3}$$

where m denotes the nonlinear order of $\Phi^{(m)}$ and M is the nonlinear order of the method which can be freely chosen. Then the surface potential and the surface vertical velocity are expanded in a Taylor series around the still water level $z = 0$

$$\begin{aligned}\Phi(x,z=\eta,t) = \phi(x,t) &= \sum_{m=1}^{M}\sum_{n=0}^{m-1} \frac{\eta^n}{n!}\frac{\partial^n \Phi^{(m-n)}}{\partial z^n}(x,z=0,t)\\ \frac{\partial \Phi}{\partial z}(x,z=\eta,t) = W(x,t) &= \sum_{m=1}^{M}\sum_{n=0}^{m-1} \frac{\eta^n}{n!}\frac{\partial^{n+1} \Phi^{(m-n)}}{\partial z^{n+1}}(x,z=0,t).\end{aligned} \tag{4}$$

For varying bottom, the bottom boundary condition

$$\frac{\partial \Phi}{\partial x}\frac{\partial \mathscr{B}}{\partial x} - \frac{\partial \Phi}{\partial z} = 0 \quad \text{at} \quad z = -h_0 + \mathscr{B}(x) \tag{5}$$

needs to be satisfied. In order to satisfy the bottom boundary condition, the velocity potential $\Phi^{(m)}$ is expressed as the sum of two velocity potentials

$$\begin{aligned}\Phi^{(m)} &= \Phi_0^{(m)} + \Phi_B^{(m)}\\ \Phi_0^{(m)}(x,z,t) &= \sum_j A_j(t)\frac{\cosh(k_j(z+h_0))}{\cosh(k_j h_0)}e^{ik_j x}\\ \Phi_B^{(m)}(x,z,t) &= \sum_j B_j(t)\frac{\sinh(k_j z)}{\cosh(k_j h_0)}e^{ik_j x}\end{aligned} \tag{6}$$

where $k_j = j\frac{2\pi}{L}$ and A_j and B_j are the modal amplitudes of $\Phi_0^{(m)}$ and $\Phi_B^{(m)}$ respectively. The velocity potential $\Phi_0^{(m)}$ is a solution of the problem for flat bottom with depth h_0 since the Neumann condition at $z = -h_0$ is satisfied:

$$\frac{\partial \Phi_0}{\partial z}(x,z=-h_0,t) = 0. \tag{7}$$

The velocity potential $\Phi_B^{(m)}$ gives correction for bottom boundary condition (5) and satisfies a Dirichlet condition at $z = 0$:

$$\Phi_B(x,z=0,t) = 0. \tag{8}$$

With velocity potential in (6) and bottom boundary condition in (5), the modal amplitudes A_j and B_j can be calculated as in Gouin, Ducrozet, and Ferrant [33] by using Taylor expansion of the bottom boundary condition around $z = -h_0$ and truncate the series to order M_B. Once the modal amplitudes A_j and B_j have been calculated, the surface velocity W can be calculated from (4). The possibility of choosing different orders, M for the free surface and M_B for the bottom, gives more flexibility to deal with cases that have different bottom variation and free surface nonlinearity.

B. Water particle kinematics calculation

The numerical method for wave evolution as described in Section II A provides the surface quantities such as surface elevation η, surface potential ϕ and surface vertical velocity W at every integration time step. For many applications, the reconstruction of kinematics inside the fluid domain is necessary. There are two methods in Bateman, Swan, and Taylor [35], the so-called H operator and the H_2 operator, to calculate the interior water particle kinematics in Dirichlet to Neumann formulation. Adaptation of these methods in HOSM formulation is given by Ducrozet *et al.* [36]. However, these methods are only valid for flat bottom. For varying bottom, we will use the kinematics calculation by Variational Boussinesq Model (VBM) as in Lawrence, Gramstad, and Trulsen [37]. Initially, VBM was introduced by Klopman, van Groesen, and Dingemans [38] for nonlinear wave propagation. Multiple works on VBM have considered the accuracy in terms of wave propagation for different cases including irregular waves propagating over varying bottom (see Klopman, van Groesen, and Dingemans [38], Adytia and van Groesen [39], Lawrence, Adytia, and van Groesen [40]). In Lawrence, Gramstad, and Trulsen [37], the VBM is adapted to reconstruct the interior wave kinematics from information of surface elevation η and velocity potential ϕ, and has been validated extensively against several test cases. The VBM for kinematics calculation is discussed briefly in the following.

In VBM, the velocity potential $\Phi(x,z,t)$ is approximated by adding z-dependent functions

$$\Phi_{VBM}(x,z,t) = \phi(x,t) + \sum_{j=1}^{P} F_j(x,z,t)\psi_j(x,t) \tag{9}$$

where F_j are vertical shape functions that will be chosen in advance, ψ_j are amplitude functions that need to be determined to satisfy the Laplace equation and P is the number of profiles. We require $\Phi_{VBM}(x,z=\eta,t) = \phi(x,t)$ and choose $F_j(x,z=\eta,t) = 0$ for any j. For the vertical shape functions, we choose the normalized hyperbolic cosine functions, called Airy profiles in Adytia and van Groesen [39]

$$F_j = \frac{\cosh[\kappa_j(z+h)]}{\cosh[\kappa_j(\eta+h)]} - 1 \tag{10}$$

where κ_j are parameters that can be optimally chosen depending on the wave field. The parameter optimization is discussed extensively in Lakhturov, Adytia, and van Groesen [41] and Lawrence, Adytia, and van Groesen [40].

The VBM solves the Laplace equation $\nabla \cdot \nabla \Phi = 0$ with Dirichlet's principle, i.e. the solution of Laplace equation is obtained by minimizing the kinetic energy. The kinetic energy of VBM is given by

$$K_{VBM} = \frac{1}{2} \int \int_{-h}^{\eta} |\nabla \Phi_{VBM}|^2 \, dz dx. \tag{11}$$

The kinetic energy minimization requires that the variational derivative of (11) with respect to ψ_j is equal to zero, $\delta_{\psi_j} K_{VBM} = 0$, leading to a system of linear elliptic equations. Then the amplitude functions ψ_j are calculated by solving these linear elliptic equations. Subsequently, the kinematics in the fluid domain can be easily calculated from (9).

III. MODEL SETUP AND VALIDATION

We simulate long-crested irregular waves propagating over varying bathymetry in a periodic computational domain $x \in [0, L]$ by HOSM. The wave generator is embedded inside the domain at $x = x_0$ as described in Liam, Adytia, and van Groesen[42]. At the left and right boundaries, damping zones with length D are implemented[39].

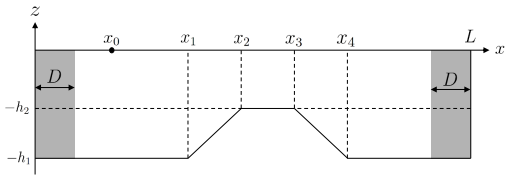

FIG. 2: Layout of computational domain.

The incoming wave field is generated by a superposition of harmonic wave components. The time series for embedded wave generation is given as

$$\eta(x = x_0, t) = \sum_{j=1}^{N} a_j \cos(\omega_j t + \varphi_j) \tag{12}$$

where $\omega_j = j\Delta\omega$ and the phases φ_j are independent random variables uniformly distributed on $[0, 2\pi)$. The amplitudes a_j are chosen deterministically based on a JONSWAP spectrum in the form

$$S(\omega) = \frac{\alpha g^2}{\omega^5} \exp\left[-\frac{5}{4}\left(\frac{\omega_p}{\omega}\right)^2\right] \gamma^{\exp\left[-\frac{(\omega-\omega_p)^2}{2\omega_p^2\sigma^2}\right]} \tag{13}$$

where σ is 0.07 for $\omega \leq \omega_p$ and 0.09 for $\omega > \omega_p$. The peak enhancement factor γ is set to 3.3 in all cases considered in this paper. The values for ω_p and α are calculated according to peak period T_p and significant wave height H_s. The number of discrete frequencies N describe the resolution of the wave spectrum and several thousands discrete frequencies are chosen to represent the spectrum in $\omega \in (0, 10\omega_p)$.

The wave kinematics are calculated by VBM as a post-processing after the HOSM simulation is finished. We repeat this set of simulations in a Monte Carlo approach where the incoming waves are generated from the same spectrum but with different random phases. From each simulation, we calculate the skewness and the kurtosis of surface elevation and horizontal velocity from time series of length $200T_p$. Note that the time series are collected after the waves have fully propagated through computational domain.

In the following we consider five sets of numerical simulations for unidirectional waves propagating over non-uniform bathymetry. First, in Section IV A, we conducted numerical simulation with the same bathymetry used in the laboratory experiment in Trulsen *et al.*[23] and the incoming wave field is generated from a JONSWAP spectrum with significant wave height $H_s = 2.5$ cm and peak period $T_p = 1.1$ s.

Then, in Section IV B, we study the effects of the significant wave height and peak period, using the same bathymetry as in Section IV A. Five different values for the significant wave height are considered, $H_s = 1.5, 2, 2.5, 3$ and 3.5 cm, all with peak period $T_p = 1.1$ s. Five different peak periods are considered, $T_p = 0.9, 1, 1.1, 1.2$ and 1.3 s, all with significant wave height $H_s = 2.5$ cm.

In Section IV C, we consider irregular waves propagating over a slope from deeper to shallower water. Here, we fix the water depths $h_1 = 0.53$ m and $h_2 = 0.11$ m and the incoming wave field with peak period $T_p = 1.1$ s and significant wave height $H_s = 2.5$ cm. The lengths of upslope is varied $L_u = 1.6, 5, 10, 15$ and 25 m which correspond to $L_u = 0.89, 2.78, 5.56, 8.34$ and $13.9\lambda_p$, respectively.

In Section IV D, we investigate irregular waves propagating over a shoal with different lengths of downslope. The water depth and incoming wave field are the same as in Section IV C. The length of the shallower part is 1.6 m. The lengths of downslope $L_d = 1.6, 3, 5, 10, 15$ m correspond to $L_d = 0.89, 1.67, 2.78, 5.56$ and $8.34\lambda_p$, respectively.

Finally in Section IV E, we investigate irregular waves propagating over a slope in a much deeper regime than in Section IV C. The incoming wave field has JONSWAP spectrum with peak period $T_p = 0.7$ s and significant wave height $H_s =$ 3.5 cm. The wave field propagates from non-dimensional depth $k_p h_1 = 4.11$ to $k_p h_2 = 1.75$. The incoming wave field needs some propagation distance in deep water to stabilize the statistical quantities. Afterwards, it propagates through an upslope with length $L_u = 3$ m .

A. Convergence study

The convergence of HOSM for varying bathymetry has been discussed extensively in Gouin, Ducrozet, and Ferrant[33,34]. Here, we give an example of convergence study for irregular waves propagating over a shoal with the same setup as in Section IV A. We set the nonlinear order of the method to $M = 3$, and we vary the order at the bottom M_b. We use $M_b = 15$ as reference solution. Figure 3 shows the time series of surface elevation at three different locations. The first one is located on the upslope, the second one is located on top of

the shoal and the last one is located on the downslope. Table I gives the root mean square error (RMSE) of surface elevation for different orders M_b relative to the reference solution, calculated over time series of length $200T_p$. We conclude that HOSM with variable depth is converging and the results obtained with $M_b = 10$ give excellent convergence with RMSE less than or equal to 0.05%.

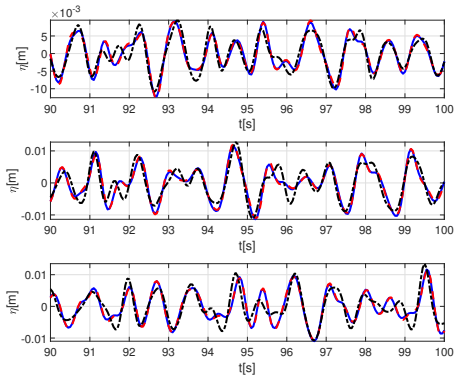

FIG. 3: Time series of surface elevation of HOSM with $M_b = 7$ (black, dashed dotted), $M_b = 10$ (red, dashed), $M_b = 15$ (blue, solid) at three different locations: on upslope (top), on top of the shoal (middle), on downslope (bottom).

TABLE I: Root mean square error of surface elevation with different nonlinear order at bottom M_b relative to $M_b = 15$ as reference solution.

M_b	RMSE		
	Upslope	Top of the shoal	Downslope
5	0.0037	0.0038	0.0043
6	0.0025	0.0021	0.0020
7	0.0017	0.0018	0.0022
8	0.0011	0.0009	0.0008
9	0.0007	0.0008	0.0009
10	0.0005	0.0004	0.0003
11	0.0003	0.0003	0.0004
12	0.0002	0.0002	0.0002

The convergence analysis of the ensemble averaged statistical quantities with respect to the number of random runs has also been conducted. As an example, Figure 4 presents the convergence of kurtosis and skewness with respect to number of runs for the experimental case in Section IV A. We found that 100 realizations is sufficient to obtain accurate estimates of the statistical quantities.

B. Mass flux in numerical simulation

There is a mass flux in the direction of wave propagation due to the difference in fluid particle velocity at crests and troughs, this effect is known as Stokes drift. The Stokes drift velocity can be defined as the difference between the average Lagrangian velocity and Eulerian velocity. An analytical solution was derived by Stokes [43]. For a harmonic wave in deep water, the Stokes drift velocity is approximately

$$\bar{u}_S \approx \omega k a^2 e^{2kz}. \tag{14}$$

In laboratory experiment, the Stokes drift will be reflected back opposite of the wave propagation direction at the end of the wave tank, we refer this as return current. When the shoal is present, there is wave reflection from the shoal itself back to the wave generator. The reflected wave will be reflected back towards the shoal by wave generator. The return current will also propagate back over the shoal towards the wave generator. It is not clear how the mass flux will be vertically distributed due to the reflection mentioned above.

In this subsection, we want to check the mass flux in the numerical simulation when the waves reach the end of computational domain through the damping zones.

We consider a linear harmonic wave propagating over flat bottom with amplitude 1 cm, period 1 s and water depth 1 m. The wave is generated at $x = 40$ m in computational domain $x \in [0, 80]$ m. The length of damping zones is 20 m. Figure 5 shows the snapshot of surface elevation at $t = 40$ s, average mass flux, and the normalized flux velocity. We show that the mass flux is due to Stokes drift and the return current is absent in our numerical simulation. This also implies that there is no reflection from the end of computational domain. It should be noted that the existence of return current in laboratory experiment may modify the wave dynamics such that the higher-order statistics are affected.

IV. RESULTS

In this section, we present numerical results from the model setup described in Section III. In all cases, we evaluate the skewness and the kurtosis of the surface elevation and also of the horizontal velocity at different z-levels. The edges of the slopes are indicated by vertical dashed lines in the figures. Table II shows the summary of our numerical cases.

A. Comparison with laboratory experiment

We present results from comparison with experiments carried out at University of Oslo, reported by Trulsen *et al.* [23]. In the experiment, the horizontal velocity measurements were made at $z = -0.048$ m. In our numerical simulation, the horizontal velocity are calculated at three different z-levels: -0.04 m, -0.06 m and -0.08 m.

Figure 6 shows the kurtosis and the skewness of surface elevation and horizontal velocity from experiments at one depth

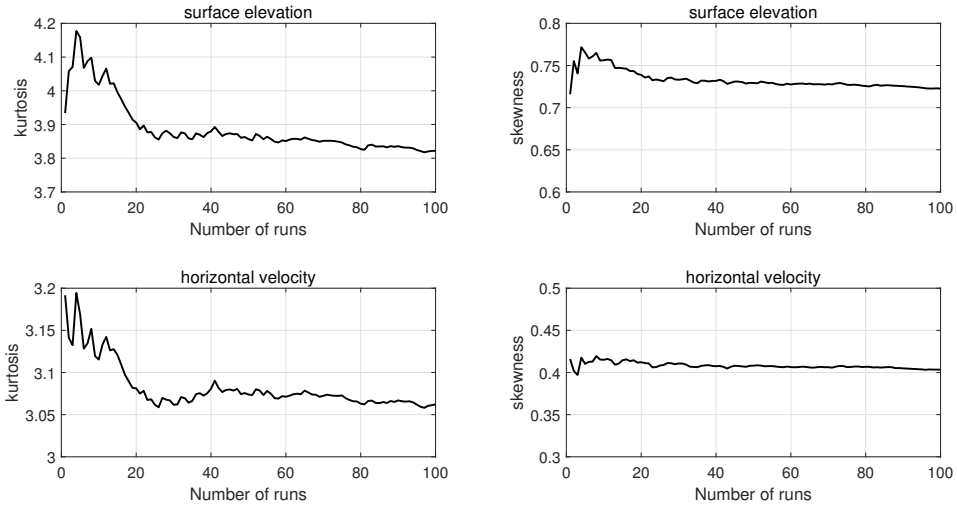

FIG. 4: Typical convergence of the ensemble-averaged kurtosis and skewness of surface elevation and horizontal velocity on top of the shoal with respect to the number of runs.

TABLE II: Summary of numerical simulations. All parameters are in SI units.

	H_s	T_p	x_1	x_2	x_3	x_4	h_1	h_2	k_ph_1	k_ph_2
Experiment	0.025	1.1	30	31.6	33.2	34.8	0.53	0.11	1.85	0.64
H_s	0.015									
	0.02									
	0.025	1.1	30	31.6	33.2	34.8	0.53	0.11	1.85	0.64
	0.03									
	0.035									
T_p		0.9							2.66	0.81
		1							2.19	0.72
	0.025	1.1	30	31.6	33.2	34.8	0.53	0.11	1.85	0.64
		1.2							1.61	0.59
		1.3							1.42	0.54
Upslope				31.6						
				35						
	0.025	1.1	30	40	100	110	0.53	0.11	1.85	0.64
				45						
				55						
Downslope						34.8				
						36.2				
	0.025	1.1	30	31.6	33.2	38.2	0.53	0.11	1.85	0.64
						43.2				
						48.2				
Deep water	0.035	0.7	60	63	100	110	0.5	0.2	4.11	1.75

and numerical simulations at various depths. Figure 7 shows the vertical variations of kurtosis and skewness of horizontal velocity from the numerical simulations. It is clearly observed that the local maximum of kurtosis and skewness of surface elevation on top of the shoal are reproduced in the numerical simulations. The skewness of the horizontal velocity has similar behaviour as the skewness of the surface elevation, while the kurtosis of horizontal velocity has its local maximum around the downslope region. The maximum kurtosis of horizontal velocity is smaller than the maximum kurtosis of surface elevation. All of these behaviours are well captured by the numerical simulations. The numerical simulations show that the kurtosis of horizontal velocity has a great variation in vertical direction just after the upslope when the kurtosis of surface elevation has local maximum. The horizontal velocity closer to still water level gives higher magnitude locally in both kurtosis and skewness. There is a deviation between experimental and numerical result in terms of the magnitude of the statistical quantities. Note that the statistics of experimental result are calculated by time averaging, meanwhile the numerical results are calculated by ensemble averaging. Additionally, the experimental results may be affected by wave reflection and return currents, which are not present in the numerical simulations as showed in Section III B. Overall, the experimental and numerical results show a good qualitative agreement.

B. The effects of significant wave height and peak period

We consider various incoming waves with different significant wave heights and peak periods propagating over the same bathymetry as in Section IV A.

Figures 8 and 9 show the kurtosis and skewness of surface elevation and horizontal velocity for different significant wave heights and peak periods, respectively. Amplification of local

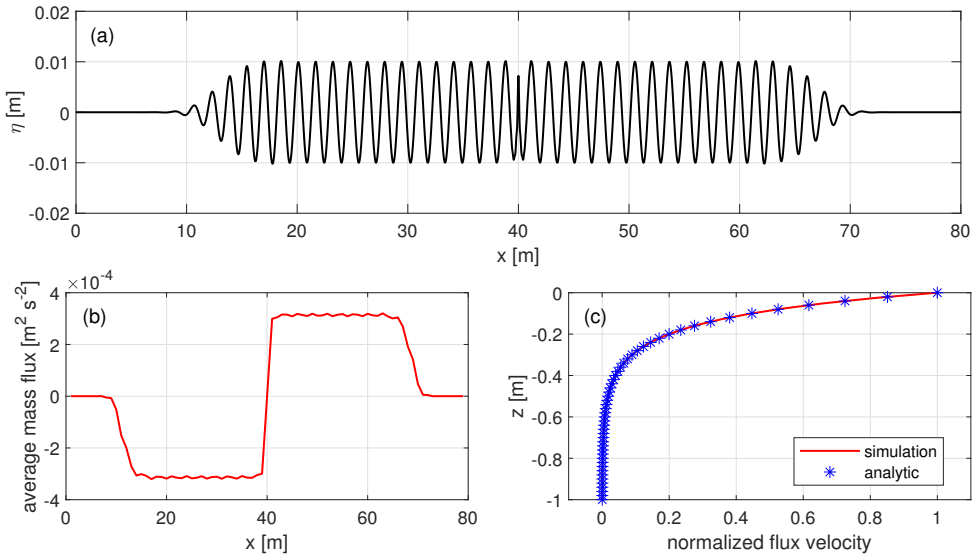

FIG. 5: (a) Snapshot of surface elevation at $t = 40$ s. (b) Vertically integrated flux, calculated by integrating the flux from bottom to $z = 0$ and averaging from $t = 40$ s to $t = 100$ s. (c) Flux velocity normalized with analytical formula of Stokes drift velocity at $z = 0$.

minimum and maximum for both kurtosis and skewness can be achieved by increasing the significant wave height. Confirming the experimental result in Trulsen *et al.* [23], there is a tendency that the location of the maximum kurtosis and skewness in surface elevation approaches the edge of the upslope of the shallower part with decreasing peak period. The local maximum of kurtosis in surface elevation starts to weaken in our case with highest non-dimensional depth $k_p h_2$. However, the local minimum and maximum of kurtosis and skewness in horizontal velocity still exist for all cases. There is also a tendency that the local minimum of the skewness of surface elevation and the local maximum of the kurtosis of horizontal velocity coincide at the same location. Furthermore, the maximum and minimum of the skewness of surface elevation are shifted to the direction of wave propagation with increasing peak period. Finally, we remark that the vertical variation of the kurtosis of horizontal velocity on top of the shoal is weakened for sufficiently low non-dimensional depth $k_p h_2$.

C. The effects of upslope length

We investigate the effects of upslope without the presence of downslope, i.e. the downslope is far enough so that the effects of upslope can be analyzed independently. Several different upslopes are considered with the same incoming waves.

Figure 10 shows the kurtosis and skewness of surface elevation and horizontal velocity with different upslope. Near the edge of the upslope in the shallower area, we observe local maximum in kurtosis and skewness of surface elevation, and then it decreases towards new statistical equilibrium. On the other hand, the kurtosis of horizontal velocity at $z = -0.08$ m has a local minimum at the same location as the local maximum of surface elevation kurtosis and it stabilizes after some distance. The skewness of horizontal velocity shows similar behaviour as the skewness of surface elevation. We notice that the local effects of kurtosis vanish when the length of upslope is sufficiently large, meanwhile the local effects of skewness are still present in our mildest case. This observation has been made in statistical quantities of surface elevation with Boussinesq model in Gramstad *et al.* [19]. Furthermore, in the shallower water regime, the kurtosis of horizontal velocity at deeper z-level is higher and it also has higher negative skewness.

D. The effects of downslope length

The results in Section IV A and IV C showed that the local maximum of kurtosis and the local minimum of skewness in horizontal velocity occurred due to the presence of a downslope. Now, we vary the downslope in Section IV A with the

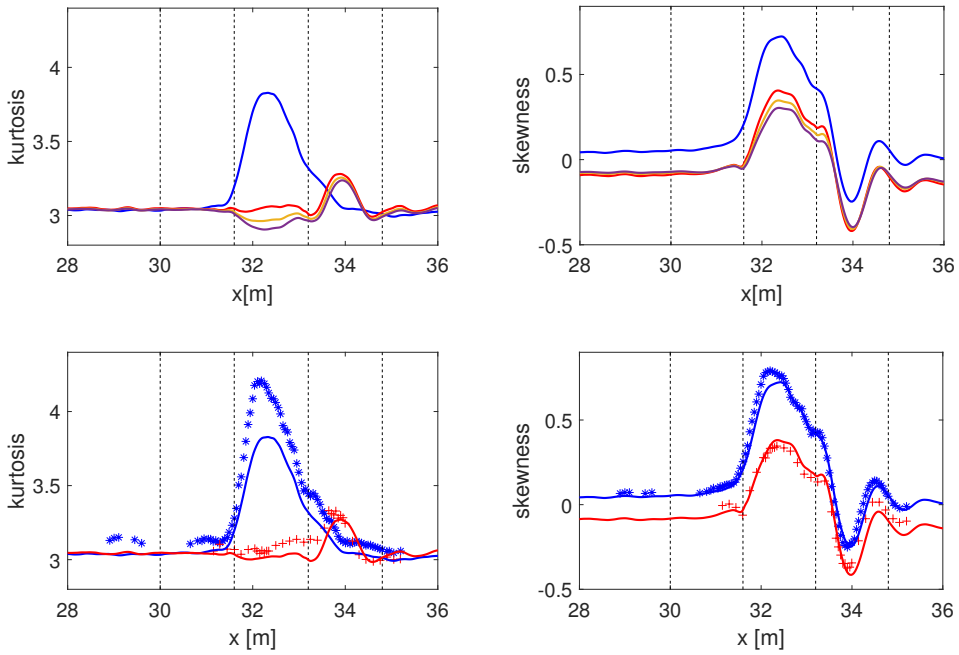

FIG. 6: Upper plot: kurtosis and skewness of surface elevation (blue) and horizontal velocity at $z = -0.04$ m (red), $z = -0.06$ m (yellow) and $z = -0.08$ m (purple) from numerical result. Lower plot: kurtosis and skewness of surface elevation (experiment: $*$, simulation: blue line) and horizontal velocity at $z = -0.048$ m (experiment: $+$, simulation: red line).

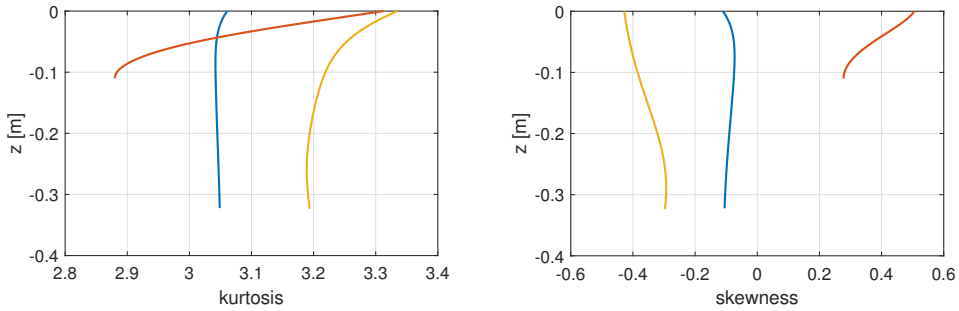

FIG. 7: Vertical variations of kurtosis and skewness of horizontal velocity on upslope area $x = 30.8$ m (blue), on top of the shoal $x = 32.4$ m (red) and on downslope area $x = 34$ m (yellow) for experimental case.

same incoming waves to study the downslope effect.

Figure 11 shows the kurtosis and skewness of surface elevation and horizontal velocity with different downslope. The local effects in the downslope area disappear as the length of downslope increases. Abrupt change of depth from shallower water to deeper water may lead to non-Gaussian statistics in horizontal velocity.

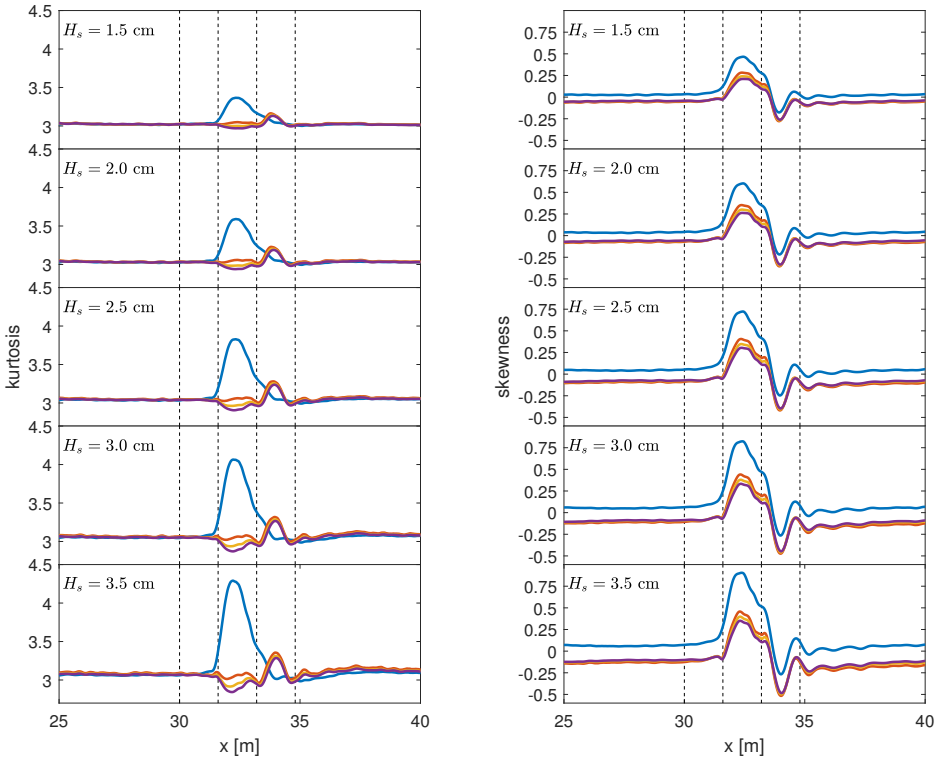

FIG. 8: Kurtosis and skewness of surface elevation (blue) and horizontal velocity at $z = -0.04$ m (red), $z = -0.06$ m (yellow) and $z = -0.08$ m (purple) for significant wave height $H_s = 1.5, 2, 2.5, 3, 3.5$ cm from top to bottom, respectively.

E. Deep water case

We consider strongly non-Gaussian waves propagating over a slope in a deeper regime where modulational instability effect is present. A similar study has been done to investigate the statistical properties of surface elevation with Nonlinear Schrödinger wave model by Zeng and Trulsen [22].

Figure 12 shows the evolution of kurtosis and skewness over a sloping bottom from non-dimensional depth $k_p h = 4.11$ to $k_p h = 1.77$. We observe transition from one statistical equilibrium to another new statistical equilibrium in shallower water.

Figure 13 shows the vertical variation of kurtosis and skewness of horizontal velocity. Towards the still water level, the kurtosis of horizontal velocity is increasing and the magnitude of skewness is increasing. In shallower water, there is a tendency that the kurtosis of horizontal velocity is increasing near the bottom and also the horizontal velocity has higher negative skewness. This observation is consistent with the results in Section IV C.

V. CONCLUSION

Numerical simulations of long-crested irregular waves propagating over a non-uniform depth have been performed using a Monte-Carlo approach to investigate the statistics of wave kinematics. Irregular waves propagating over a sufficiently shallow shoal have a local maximum of the kurtosis and skewness of surface elevation near the edge of the upslope on the shallower part of the shoal. As pointed out in the experimental result of Trulsen *et al.* [23], the corresponding horizontal velocity has a local maximum of kurtosis on the downslope area and the local maximum of skewness is achieved at the same location as the surface elevation. Our numerical results are in qualitative agreement with the experimental result of Trulsen *et al.* [23].

The effects of significant wave height and peak period are investigated. The local effects of kurtosis and skewness for

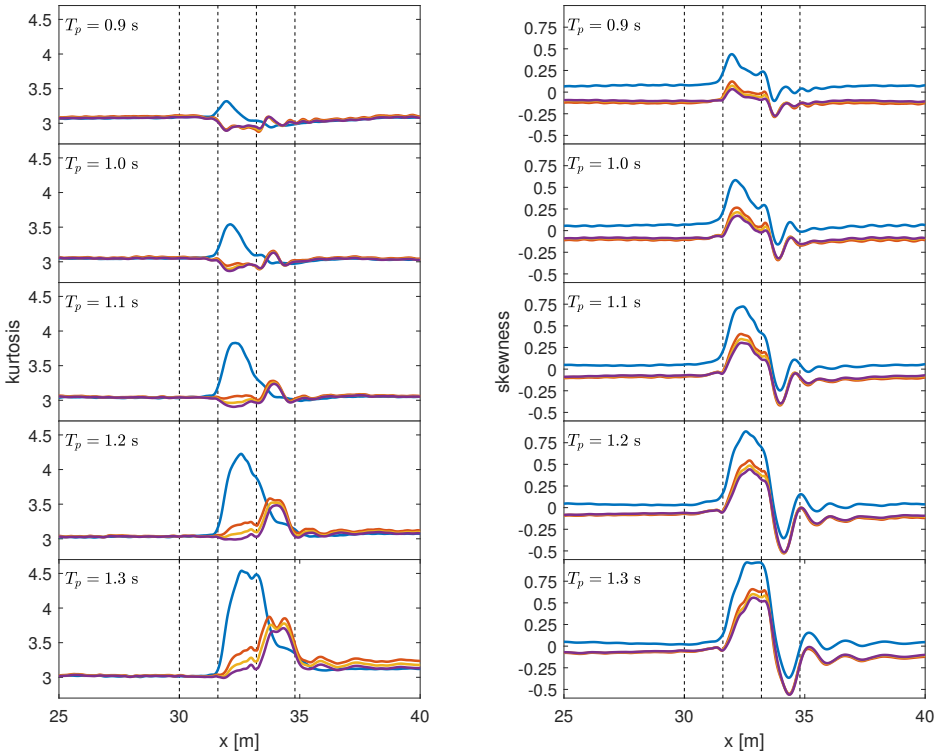

FIG. 9: Kurtosis and skewness of surface elevation (blue) and horizontal velocity at $z = -0.04$ m (red), $z = -0.06$ m (yellow) and $z = -0.08$ m (purple) for peak period $T_p = 0.9, 1, 1.1, 1.2, 1.3$ s from top to bottom, respectively.

both surface elevation and horizontal velocity can be amplified by increasing the significant wave height or increasing the peak period. In other words, this physical phenomenon only occurs in high sea states in sufficiently shallow water.

The skewness and kurtosis of the surface elevation have local maxima due to the upslope. We found that the kurtosis of the horizontal velocity has a strong vertical variation where the kurtosis of surface elevation reach its maximum. Meanwhile, the downslope length is responsible for local maximum of kurtosis in horizontal velocity. All of these local effects can vanish when the bottom slope becomes milder.

It has previously been shown in Zeng and Trulsen [22] with Nonlinear Schrödinger model that in a deeper regime with modulational instability, the slope connects two different statistical equilibriums of surface elevation. In the transition region, there is no local maximum of skewness and kurtosis. Our results are in agreement with the results in Zeng and Trulsen [22]. While it has still not been confirmed by experimental measurements, this is the first verification of their results by means of a highly nonlinear numerical model. The statistical properties of horizontal velocity also show the same behaviour as the surface elevation. Furthermore, the vertical variation of skewness and kurtosis in horizontal velocity in shallower water shows that the kurtosis is higher and it has higher negative skewness near the mean water level and the bottom.

DATA AVAILABILITY

The data that support the findings of this study are available from the corresponding author upon reasonable request.

ACKNOWLEDGMENTS

We thank anonymous referees for valuable comments. The experimental data were kindly made available in Trulsen *et al.* [23].

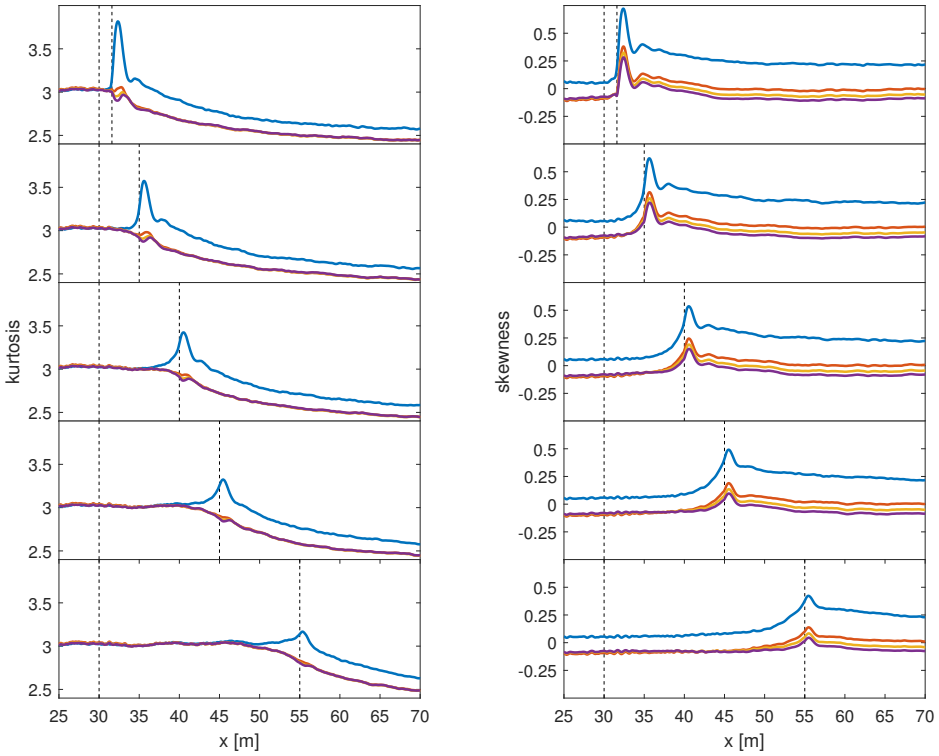

FIG. 10: Kurtosis and skewness of surface elevation (blue) and horizontal velocity at $z = -0.04$ m (red), $z = -0.06$ m (yellow) and $z = -0.08$ m (purple) for different length of upslope.

[1]J. Morison, J. Johnson, and S. Schaaf, "The force exerted by surface waves on piles," Journal of Petroleum Technology **2**, 149–154 (1950).
[2]R. G. Dean and R. A. Dalrymple, *Water Wave Mechanics for Engineers and Scientists*, Advanced Series on Ocean Engineering, Vol. 2 (World Scientific, Singapore, 1991).
[3]B. M. Sumer and J. Fredsøe, *The Mechanics of Scour in the Marine Environment*, Advanced Series on Ocean Engineering, Vol. 17 (World Scientific, Singapore, 2002).
[4]Y. Goda, *Random Seas and Design of Maritime Structures*, Advanced Series on Ocean Engineering, Vol. 33 (World Scientific, Singapore, 2010).
[5]J. N. Sharma and R. G. Dean, "Second-order directional seas and associated wave forces," Society of Petroleum Engineers Journal **21**, 129–140 (1981).
[6]G. Z. Forristall, "Wave crest distributions: Observations and second-order theory," *Journal of Physical Oceanography*, J. Phys. Oceanogr. **30**, 1931–1943 (2000).
[7]P. A. E. M. Janssen and M. Onorato, "The intermediate water depth limit of the Zakharov equation and consequences for wave prediction," J. Phys. Oceanogr. **37**, 2389–2400 (2007).
[8]M. K. Ochi, *Ocean Waves The Stochastic Approach*, Cambridge Ocean Technology series; 6 (Cambridge, 1998).
[9]E. M. Bitner, "Non-linear effects of the statistical model of shallow-water wind waves," Applied Ocean Research **2**, 63–73 (1980).
[10]Z. Cherneva, P. Petrova, N. Andreeva, and C. Guedes Soares, "Probability distributions of peaks, troughs and heights of wind waves measured in the black sea coastal zone," Coastal Engineering **52**, 599–615 (2005).
[11]K. Trulsen, H. Zeng, and O. Gramstad, "Laboratory evidence of freak waves provoked by non-uniform bathymetry," Phys. Fluids **24**, 097101 (2012).
[12]Y. Ma, G. Dong, and X. Ma, "Experimental study of statistics of random waves propagating over a bar," Coastal Engineering Proceedings **1**, 30 (2014).
[13]H. Kashima, K. Hirayama, and N. Mori, "Estimation of freak wave occurrence from deep to shallow water regions," Coastal Engineering Proceedings **1**, 36 (2014).
[14]C. T. Bolles, K. Speer, and M. N. Moore, "Anomalous wave statistics induced by abrupt depth change," Physical review fluids **4**, 011801 (2019).
[15]J. Zhang, M. Benoit, O. Kimmoun, A. Chabchoub, and H.-C. Hsu, "Statistics of extreme waves in coastal waters: Large scale experiments and advanced numerical simulations," Fluids **4**, 1–24 (2019).
[16]A. Sergeeva, E. Pelinovsky, and T. Talipova, "Nonlinear random wave field in shallow water: variable Korteweg-de Vries framework," Nat. Hazards Earth Syst. Sci. **11**, 323–330 (2011).
[17]A. J. Majda, M. N. J. Moore, and D. Qi, "Statistical dynamical model to predict extreme events and anomalous features in shallow water waves with abrupt depth change," Proc. Natl. Acad. Sci. **116**, 3982–3987 (2019).
[18]N. Moore, C. Bolles, A. Majda, and D. Qi, "Anomalous waves triggered by abrupt depth changes: Laboratory experiments and truncated KdV statistical mechanics," J Nonlinear Sci **30**, 3235–3263 (2020).

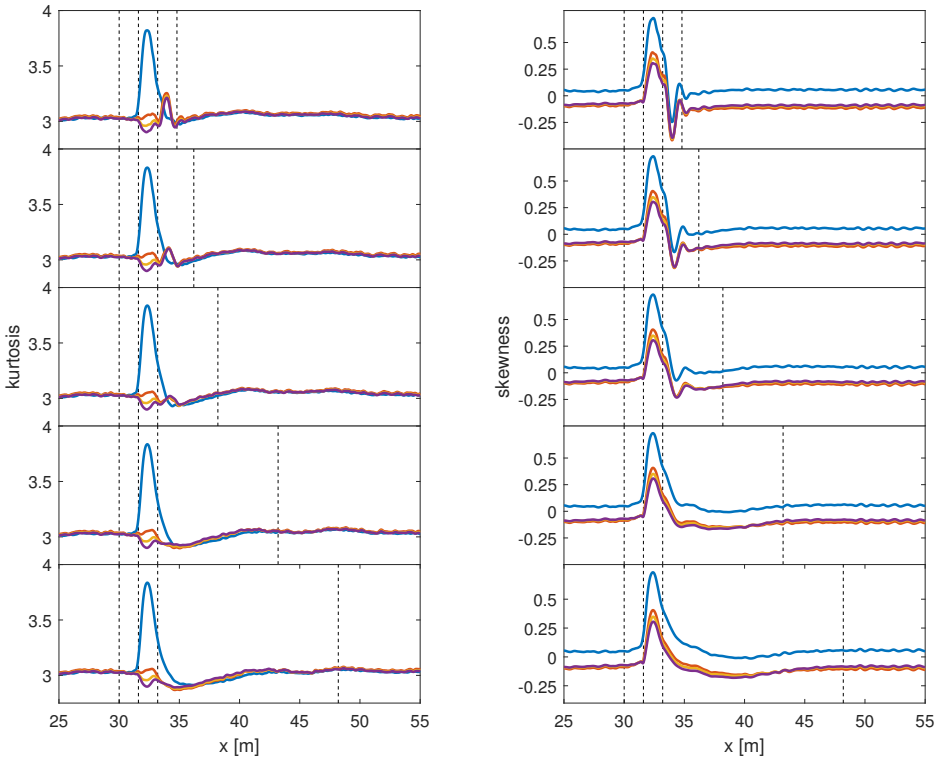

FIG. 11: Kurtosis and skewness of surface elevation (blue) and horizontal velocity at $z = -0.04$ m (red), $z = -0.06$ m (yellow) and $z = -0.08$ m (purple) for different length of downslope.

[19]O. Gramstad, H. Zeng, K. Trulsen, and G. K. Pedersen, "Freak waves in weakly nonlinear unidirectional wave trains over a sloping bottom in shallow water," Phys. Fluids **25** (2013).
[20]Y. Zheng, Z. Lin, Y. Li, T. Adcock, Y. Li, and T. van den Bremer, "Fully nonlinear simulations of unidirectional extreme waves provoked by strong depth transitions: The effect of slope," Physical Review Fluids **5**, 064804 (2020).
[21]C. Viotti and F. Dias, "Extreme waves induced by strong depth transitions: Fully nonlinear results," Physics of Fluids **26**, 051705 (2014).
[22]H. Zeng and K. Trulsen, "Evolution of skewness and kurtosis of weakly nonlinear unidirectional waves over a sloping bottom," Natural Hazards and Earth System Sciences **12**, 631–638 (2012).
[23]K. Trulsen, A. Raustl, S. Jorde, and L. B. Rye, "Extreme wave statistics of long-crested irregular waves over a shoal," Journal of Fluid Mechanics **882**, R2 (2020).
[24]G. Ducrozet and M. Gouin, "Influence of varying bathymetry in rogue wave occurrence within unidirectional and directional sea-states," Journal of Ocean Engineering and Marine Energy (2017).
[25]C. C. Tung, "Statistical properties of the kinematics and dynamics of a random gravity wave field," J. Fluid Mech. **70**, 251–255 (1975).
[26]W. Cieslikiewicz and O. T. Gudmestad, "Stochastic characteristics of orbital velocities of random water waves," J. Fluid Mech. **255**, 275–299 (1993).
[27]J. B. Song and Y. H. Wu, "Statistical distribution of water-particle velocity below the surface layer for finite water depth," Coastal Engineering **40**, 1–19 (2000).
[28]A. Alberello, A. Chabchoub, O. Gramstad, A. V. Babanin, and A. Toffoli, "Non-Gaussian properties of second-order wave orbital velocity," Coastal Engineering **110**, 42–49 (2016).
[29]V. E. Zakharov, "Stability of periodic waves of finite amplitude on the surface of a deep fluid," J. Appl. Mech. Tech. Phys. **9**, 190–194 (1968).
[30]D. G. Dommermuth and D. K. P. Yue, "A high-order spectral method for the study of nonlinear gravity waves," J. Fluid Mech. **184**, 267–288 (1987).
[31]B. J. West, K. A. Brueckner, R. S. Janda, D. M. Milder, and R. L. Milton, "A new numerical method for surface hydrodynamics," J. Geophys. Res. **92**, 11803–11824 (1987).
[32]Y. M. Liu and D. K. P. Yue, "On generalized Bragg scattering of surface waves by bottom ripples," Journal of Fluid Mechanics **356**, 297–326 (1998).
[33]M. Gouin, G. Ducrozet, and P. Ferrant, "Development and validation of a non-linear spectral model for water waves over variable depth," European Journal of Mechanics - B/Fluids **57**, 115–128 (2016).
[34]M. Gouin, G. Ducrozet, and P. Ferrant, "Propagation of 3D nonlinear waves over an elliptical mound with a high-order spectral method," European Journal of Mechanics - B/Fluids **63**, 9–24 (2017).
[35]W. J. D. Bateman, C. Swan, and P. H. Taylor, "On the calculation of the water particle kinematics arising in a directionally spread wavefield," J. Comput. Phys. **186**, 70–92 (2003).

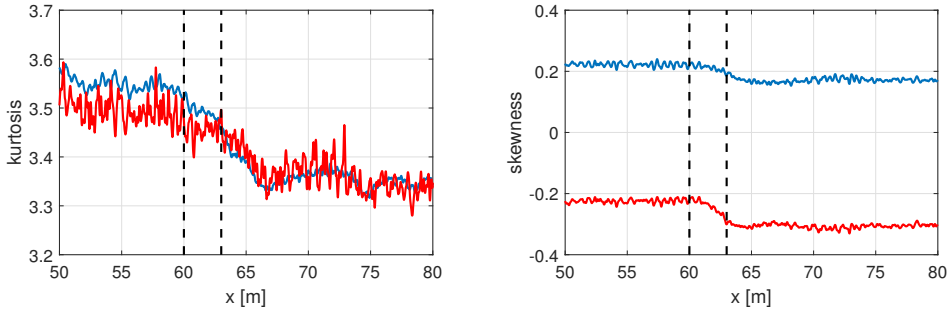

FIG. 12: Kurtosis and skewness of surface elevation (blue) and horizontal velocity at $z = -0.1$ m (red) for numerical case in deeper regime.

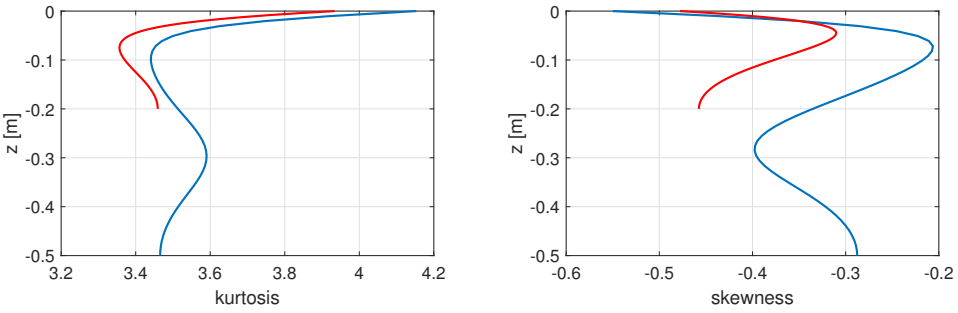

FIG. 13: Vertical variations of kurtosis and skewness of horizontal velocity before the upslope at $x = 50$ m (blue) and after the upslope $x = 70$ m (red) for numerical case in deeper regime.

[36]G. Ducrozet, F. Bonnefoy, D. Le Touzé, and P. Ferrant, "HOS-ocean: Open-source solver for nonlinear waves in open ocean based on High-Order Spectral method," Computer Physics Communications **203**, 245–254 (2016).
[37]C. Lawrence, O. Gramstad, and K. Trulsen, "Variational Boussinesq model for kinematics calculation of surface gravity waves over bathymetry," Wave Motion **100**, 102665 (2021).
[38]G. Klopman, E. van Groesen, and M. W. Dingemans, "A variational approach to boussinesq modeling of fully non-linear water waves," J. Fluid Mech **657**, 36–63 (2010).
[39]D. Adytia and E. van Groesen, "Optimized Variational 1D Boussinesq modelling of coastal waves propagating over a slope," Coastal Eng. **64**, 139–150 (2012).
[40]C. Lawrence, D. Adytia, and E. van Groesen, "Variational Boussinesq model for strongly nonlinear dispersive waves," Wave Motion **76**, 78–102 (2018).
[41]I. Lakhturov, D. Adytia, and E. van Groesen, "Optimized Variational 1D Boussinesq modelling for broad-band waves over flat bottom," Wave Motion **49**, 309–322 (2012).
[42]L. S. Liam, D. Adytia, and E. van Groesen, "Embedded wave generation for dispersive surface wave models," Ocean Engineering **80**, 73 – 83 (2014).
[43]G. G. Stokes, "On the theory of oscillatory waves," Trans. Camb. Philos. Soc. **8**, 441–455 (1847).

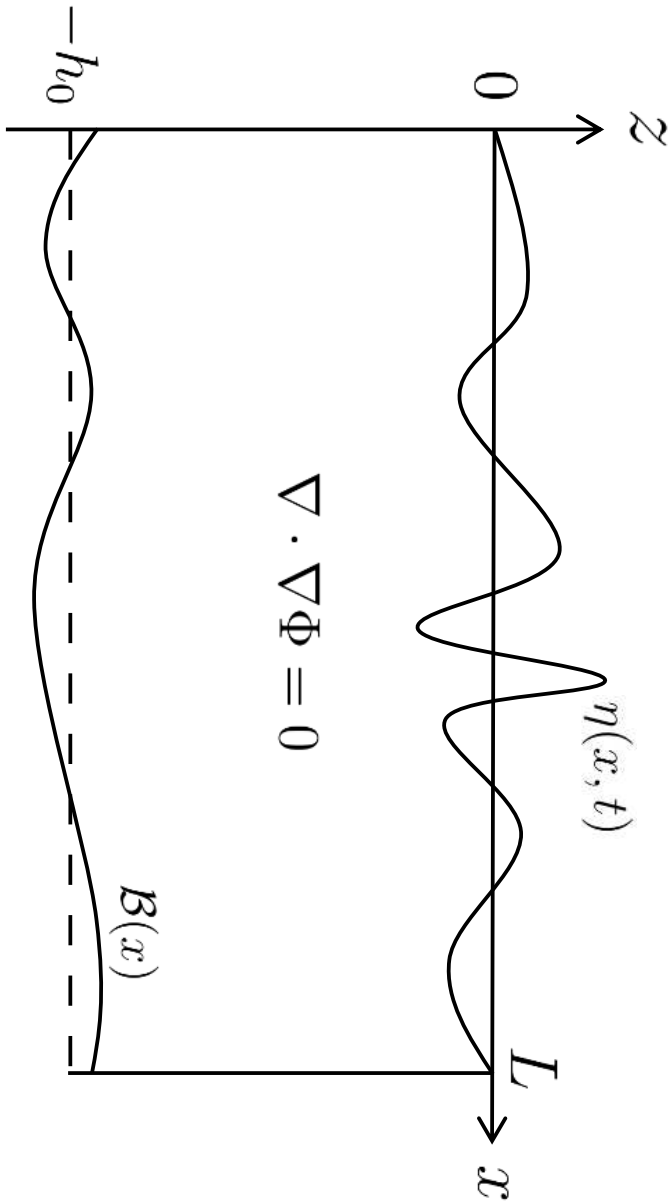

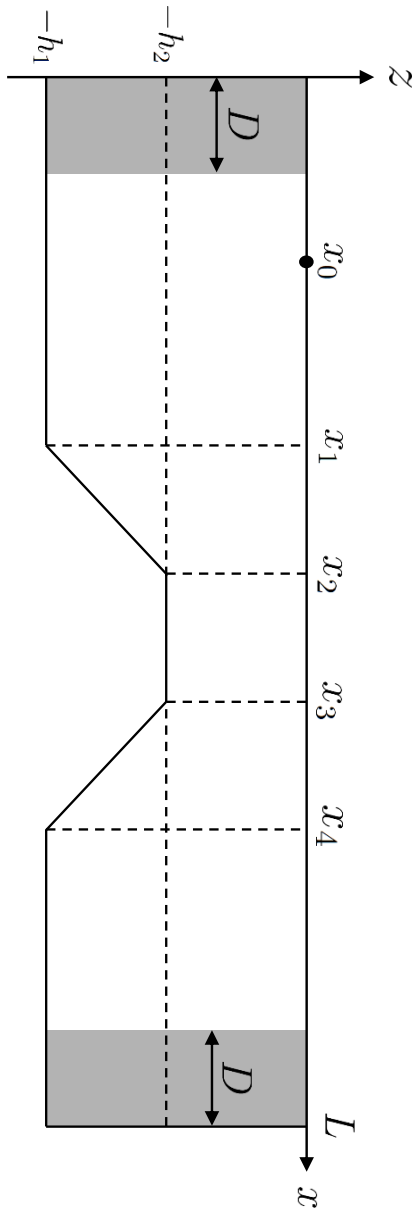

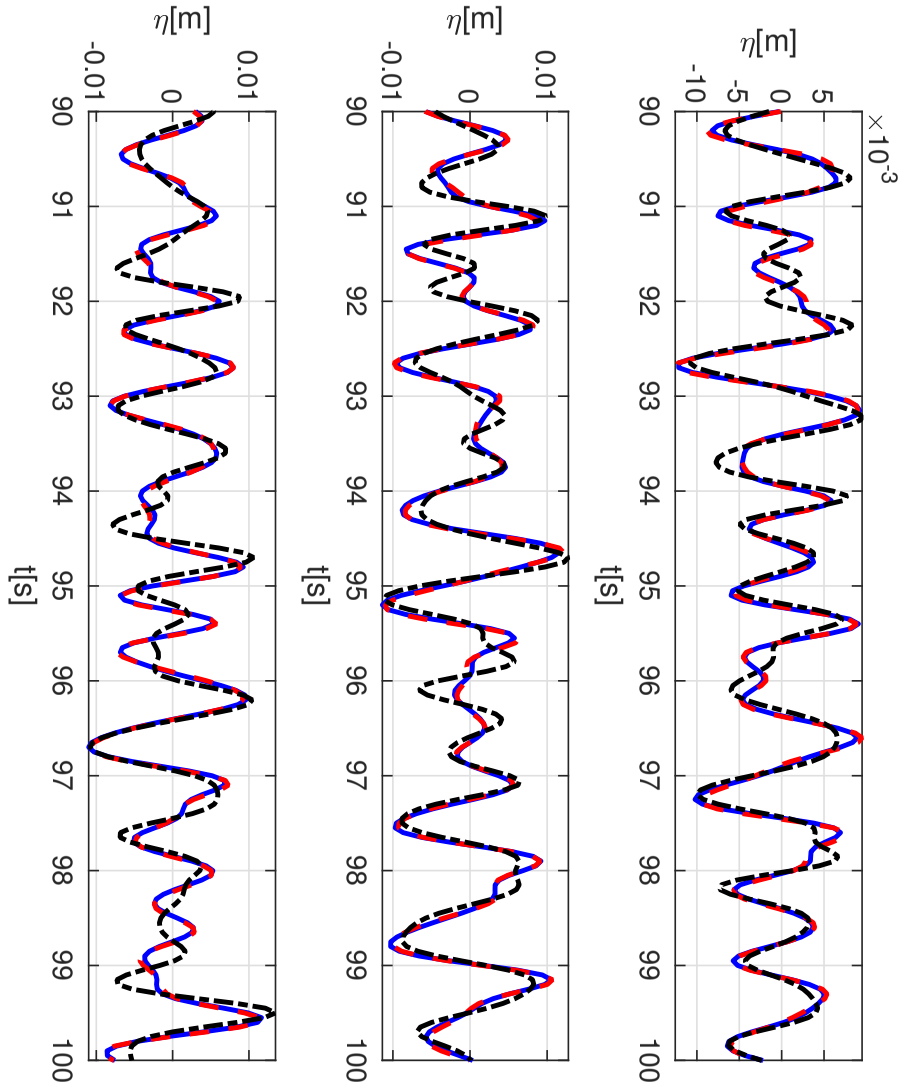

PLEASE CITE THIS ARTICLE AS DOI: 10.1063/5.0047643

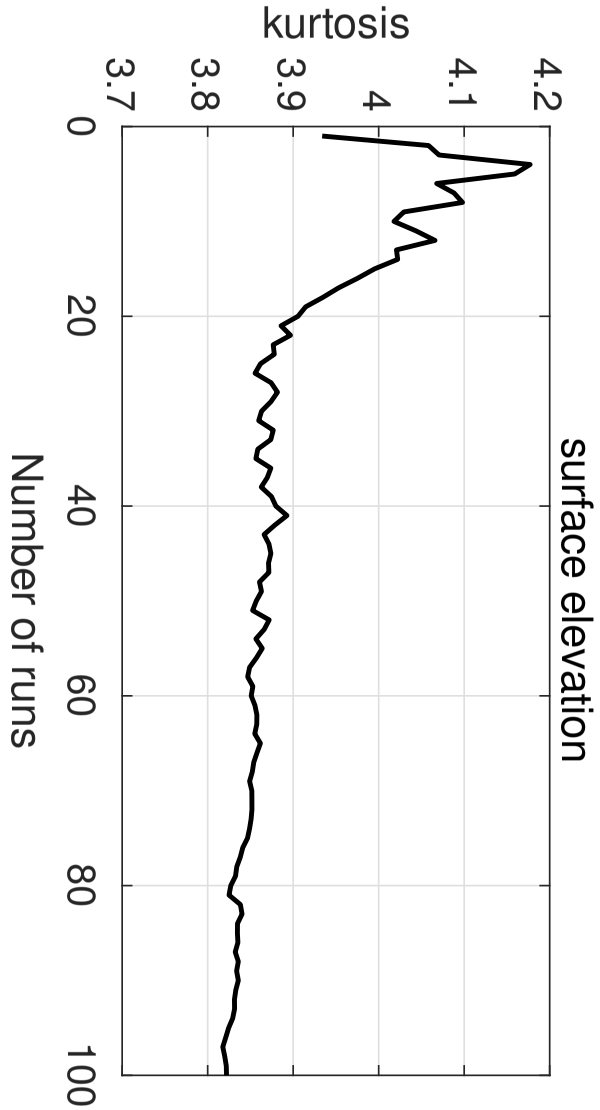

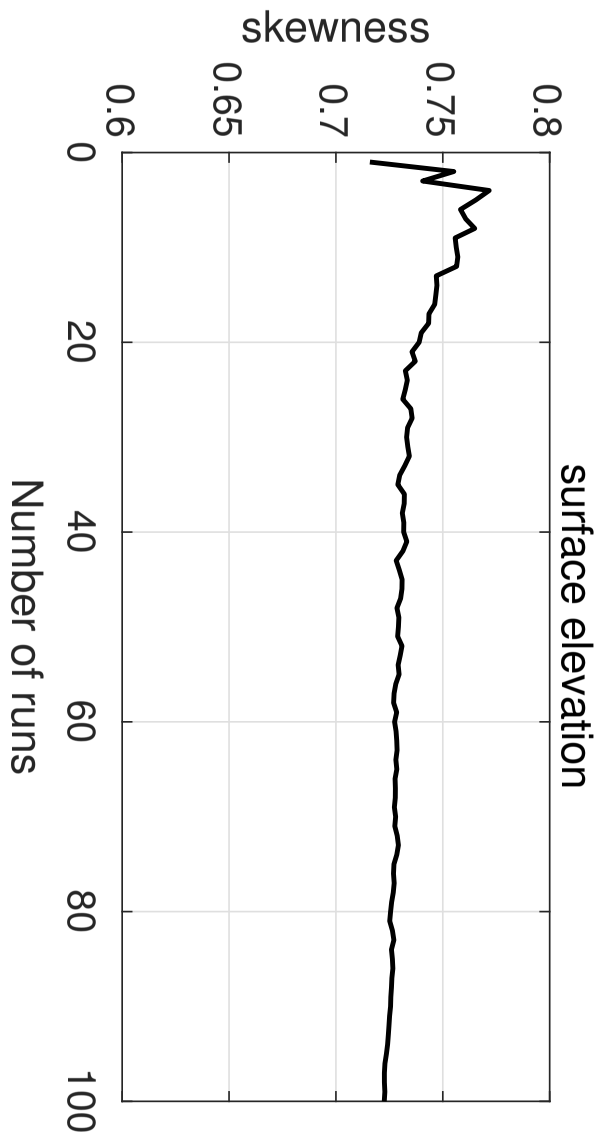

PLEASE CITE THIS ARTICLE AS DOI: 10.1063/5.0047643